Composition of III-V ternary materials under arbitrary material fluxes: The general approach unifying kinetics and thermodynamics

Vladimir G. Dubrovskii[1,*] and Egor D. Leshchenko[2]

[1]*Faculty of Physics, Saint Petersburg State University, Universitetskaya Embankment 13B, 199034 Saint Petersburg, Russia*

[2]*Submicron Heterostructures for Microelectronics, Research and Engineering Center RAS, Politekhnicheskaya Street 26, 194021 Saint Petersburg, Russia*

(Received 17 May 2023; accepted 30 June 2023; published 14 July 2023)

Understanding and controlling the composition of III-V ternary nanomaterials is essential for band-gap tunability and fabrication of functional nanoheterostructures. The kinetic approach developed so far is based on the assumption of *C*-rich growth of a ternary $A_xB_{1-x}C$ material based on intermix of *A* and *B* atoms. This holds for epilayers based on group III intermix, but is not true for epilayers based on group V intermix or vapor-liquid-solid nanowires based on group III intermix. Herein, we develop a general growth theory and obtain a vapor-solid distribution which described the ternary composition under arbitrary material fluxes and for any III-V material. This vapor-solid distribution is a combination of the kinetic and equilibrium distributions, whose weights depend on the ratio ε of the total flux of *A* and *B* atoms over the flux of *C* atoms. At $\varepsilon \ll 1$, the composition is kinetically controlled, while at $\varepsilon \gg 1$ it becomes thermodynamically limited even at infinitely high binary supersaturations for *AC* and *BC* pairs. The model fits very well the compositional data on the $InSb_xAs_{1-x}$ epilayers, $AlSb_xAs_{1-x}$ epilayers, and $InSb_xAs_{1-x}$ nanowires under different total V/III flux ratios. It reveals some fundamental properties of the vapor-solid distribution beyond the assumption of decoupled binary fluxes. In particular, the vapor-solid distribution becomes purely thermodynamic and presents the miscibility gap below the critical temperature under *AB*-rich conditions for an $A_xB_{1-x}C$ ternary regardless of the vapor supersaturation. The miscibility gap can be fully circumvented in the *C*-rich regime, where the solid composition is driven by the kinetic factors.

DOI: 10.1103/PhysRevMaterials.7.074603

I. INTRODUCTION

Compositional control over ternary III-V and III-nitride nanomaterials is essential for band-gap engineering and fabrication of functional heterostructures based on such materials [1–3]. Stoichiometric or pseudobinary III-V solids $A_xB_{1-x}C = (AC)_x(BC)_{1-x}$ based on either group III (with *A* and B atoms belonging to group III and *C* atoms belonging to group V) or group V (with *A* and *B* atoms belonging to group V and *C* atoms belonging to group III) intermix are grown from atomic vapor fluxes I_A, I_B, and I_C. The vapor-solid distribution $x(z)$ for a given material system and nanostructure geometry links the solid composition to the content of *A* atoms in vapor, $z = I_A/(I_A + I_B)$ at a given temperature *T* and the total flux ratio $\varepsilon = (I_A + I_B)/I_C$. The vapor-solid distribution fully characterizes the composition of a ternary material versus the technologically controlled vapor fluxes. The vapor-solid distributions of ternary epilayers based on group III [4–8] and group V [8–14] intermix were studied in great detail and modeled using different approaches including thermodynamic models [4–8,10–12], kinetic models for the vapor-solid incorporation [9,10,13,14], and their combination [10]. Most of these models, with only one exception [10], disregard the influence of the total flux ratio ε on the solid composition, while it was shown to change very significantly the vapor-solid distributions of $InSb_xAs_{1-x}$ [10] and $AlSb_xAs_{1-x}$ [12] epilayers. In both material systems, the compositions of epilayers grown at a V/III flux ratio of about unity were close to the linear dependence $x = z$, while at large V/III ratios they featured nonlinear shapes in which the Sb fraction in a solid was greatly reduced. The seminal work of Biefeld [10] remains, to our knowledge, the only approach enabling a systematic treatment of the total V/III ratio dependence of the solid composition. It is restricted, however, to the case of III-Sb_xAs_{1-x} ternaries and requires numerical solution of the four coupled equations describing the reaction-limited growth kinetics at the surface.

Ternary III-V nanowires and heterostructures based on such nanowires offer an almost unlimited flexibility in band-gap engineering and coherent growth on dissimilar substrates such as Si [15–19]. Freestanding ternary III-V nanowires can be fabricated by different deposition techniques including molecular beam epitaxy (MBE) and vapor phase epitaxy (VPE) via the catalyst-free vapor-solid growth mechanism (often in selective area growth on patterned substrates) or the vapor-liquid-solid (VLS) growth mechanism with different metal catalysts (often Au or a group III metal in the self-catalyzed approach) [18,19]. The compositions of vapor-solid ternary nanowires and nanowire heterostructures based on group III [20–22] and group V [23–25] intermix, and VLS nanowires based on group III [26–33] and group V [33–38] intermix, revealed some trends which are specific for the vertical nanowire geometry. In particular, the vapor-solid distributions

*Corresponding author: dubrovskii@mail.ioffe.ru

of Au-catalyzed $Al_xGa_{1-x}As$ nanowires were dependent on the effective diffusion lengths of Al and Ga adatoms on the nanowire sidewalls [33], the morphology and even the crystal phase (cubic zinc blende or hexagonal wurtzite) of ternary III-V nanowires in different material systems were influenced by their composition [24,26,30,33,36,38], and the interfacial abruptness in axial nanowire heterostructures was affected by the reservoir effect in a catalyst droplet [32,38]. Importantly, no miscibility gaps were present in the experimental vapor-solid distributions of $In_xGa_{1-x}As$ [30,31] and $In_xGa_{1-x}N$ [21] nanowires below the critical temperatures for these materials, which was explained by the kinetic suppression of thermodynamic factors at high enough vapor supersaturations [21].

A large amount of the available compositional data obtained for different material systems and epitaxy techniques stimulated rapid development of the compositional modeling of ternary III-V nanowires (see, for example, Refs. [38–40] for comprehensive reviews). In the most complex case of Au-catalyzed VLS nanowires, ternary islands or fractional monolayers grow at the liquid-solid interface from the liquid phase in a catalyst droplet, which is a quaternary Au-*A*-*B*-*C* melt with concentrations c_A, c_B, and c_{Au} for atoms *A*, *B*, and Au, respectively, and $1 - c_A - c_B - c_{Au}$ for atom *C*. Consequently, most models of VLS ternary nanowires treated the liquid-solid distributions $x(y)$, where $y = c_A/(c_A + c_B)$ in the *A* content in liquid [41–45,47–49]. Many fewer works tried to link the nanowire composition to the vapor fluxes [31,35,46,49,50]. The vapor-solid distributions of Au-catalyzed $InSb_xAs_{1-x}$ nanowires of Ref. [35] were modeled using the scheme of Biefeld [10], where the actual V/III ratio for fluxes entering the droplets was largely reduced with respect to their nominal values in vapor due to surface diffusion of In adatoms to the droplets. While the liquid-solid distributions can have little influence on the steady state composition of III-V ternary nanowires under constant vapor fluxes [33,46,50], they are essential for studying the time-dependent reservoir effect on the interfacial abruptness [32,42,49]. Regardless of the nature of the mother phase (liquid or vapor) feeding a III-V ternary solid, the existing approaches for compositional modeling can be divided into equilibrium [4–8,10,12,41], nucleation limited [42–45], and kinetic [10,31,46–50]. The comprehensive kinetic models contain thermodynamically controlled regimes (equilibrium or nucleation limited) in the limiting cases [10,47,48,50].

The two-parametric equilibrium or purely thermodynamic vapor-solid distribution is given by [50]

$$z = \frac{1}{1 + f(x)},$$
$$f(x) = \beta_0 \frac{(1-x)}{x} e^{\omega(2x-1)},$$
$$\beta_0 = \frac{\tau_A}{\tau_B} \frac{(n_B n_C)^{eq}}{(n_A n_C)^{eq}}. \quad (1)$$

Here, β_0 is a thermodynamic parameter given by the ratio of the binary equilibrium constants for the vapor-solid incorporation of *BC* and *AC* pairs ($(n_B n_C)^{eq}/\tau_B$ and $(n_A n_C)^{eq}/\tau_A$ [11] in the notations used in this paper, with $(n_k n_C)^{eq}$ as the equilibrium activity of a *kC* pair of atoms at the island boundary and τ_k as the desorption-limited lifetime of adatoms *k* (for $k = A, B$), and ω as the pseudobinary interaction constant of *AC* and *BC* pairs in a solid in thermal units of k_BT. The parameter ω may depend on *x* if higher order interactions in a solid are included [6,7,43–45,49]. The nucleation-limited liquid-solid distribution for VLS III-V ternary nanowires obtained in Ref. [42] has a similar form, with *y*-dependent β_0. The equilibrium distribution is independent of the vapor fluxes I_A, I_B, and I_C and binary supersaturations for *AC* and *BC* pairs. It presents the miscibility gap whenever $\omega > 2$, which disappears above the critical temperature corresponding to $\omega_c = 2$.

The most general form of the kinetically controlled vapor-solid distribution obtained in Ref. [50] for a variety of nanostructure geometries has the form

$$z = \frac{x}{c + (1-c)x}[1 + \Gamma(1-x)(ce^{\omega(1-x)^2} - \beta_0 e^{\omega x^2})],$$
$$c = \frac{\Lambda_A}{\Lambda_B},$$
$$\Gamma = \frac{(n_A n_C)^{eq}}{I_C(I_A + I_B)\tau_A \tau_C}. \quad (2)$$

This formula is four-parametric and contains two additional parameters relative to Eq. (1). The kinetic parameter *c* is given by the ratio of the effective collection lengths of *A* and *B* adatoms and describes the possible difference in the areas from which these adatoms are collected by a growing ternary solid (for example, different collection lengths on the sidewalls of vertical nanowires [33,50]). The parameter Γ at a fixed total flux of *A* and *B* atoms, $I_{tot} = I_A + I_B$, is related to the binary vapor supersaturation for *AC* pairs, and decreases for larger fluxes I_{tot} and I_C. The kinetic liquid-solid distribution obtained in Refs. [47–49] has the same form as Eq. (2), with *y*-dependent coefficients β_0 and Γ. The kinetic distribution given by Eq. (2) also contains the miscibility gaps at $\omega > 2$, which enters differently compared to Eq. (1) and disappears regardless of the growth temperature when $\Gamma \to 0$, i.e., at high supersaturations of a mother phase. This property was used, for example, in Refs. [21,47–50] to explain the kinetic suppression of the miscibility gaps in InGaAs and InGaN material systems. Without the Γ term, Eq. (2) is reduced to the Langmuir-McLean formula [51], used in many works for modeling the vapor-solid distribution of III-V ternary epilayers [9,52] and nanowires [23,33]. At $c = 1$, the Langmuir-McLean distribution is further reduced to $x = z$. This kinetic distribution shows that, in the absence of any rejected material fluxes, the solid composition is simply determined by the ratio of the incoming vapor fluxes of *A* and *B* atoms.

As pointed out in Ref. [50], the kinetic distribution given by Eq. (2) applies only under *C*-rich growth conditions for an $A_xB_{1-x}C$ ternary, where the growth is controlled by the diffusion fluxes of adatoms *A* and *B* in the excess of *C* atoms, which are readily available for crystallization at the growth interface. According to Ref. [50], the growth modeling under *C*-rich conditions is reduced to the one-component approximation for surface diffusion of *A* and *B* adatoms, while a spatially uniform concentration of adatoms *C* is determined by the balance of their arrival and desorption rates and enters the resulting distribution as an external parameter. *C*-rich growth conditions hold in most cases for $A_xB_{1-x}C$ epilayers [1,4,5,50]

and vapor-solid nanowires [21] based on group III intermix. Indeed, *AB*-rich conditions in this case would lead to the formation of *A*-*B* liquid around the growth interface, rendering the growth into the conditions of liquid phase epitaxy. This corresponds to the case of VLS $A_xB_{1-x}C$ nanowires. Highly volatile group V atoms are present in the droplets at extremely low concentrations (typically on the order of 0.01 [19]), which is why the VLS growth of III-V ternary nanowires cannot proceed under group V rich conditions, as described by Eq. (2). Similarly, the vapor-solid growth of III-V ternary solids based on group V intermix cannot be group III rich without forming a group III liquid around a growing solid, and hence cannot be described by the kinetic model given by Eq. (2). This model should be directly applicable for vapor-solid ternaries based on group III intermix or VLS nanowires based on group V intermix, while other cases require a generalization of the model for arbitrary material influxes. Furthermore, the "kinetic suppression" of thermodynamic factors including the miscibility gaps based on Eq. (2) is not always valid. The binary supersaturation can be increased, for example, by raising the total flux of *A* and *B* atoms $I_{\text{tot}} = I_A + I_B$ at a constant I_C in such a way that $\Gamma \to 0$, which would result in the purely kinetic Langmuir-McLean formula according to Eq. (2). However, this conclusion is wrong, because Eq. (2) is not valid under *C*-poor conditions.

On a more general ground, the kinetic models of Refs. [21,47–50] use a simplified growth picture in which the $A_xB_{1-x}C$ solid attaches and emits *AC* and *BC* pairs. This is certainly valid for the emission processes, because a stoichiometric solid consists of *AC* and *BC* pairs and can only emit them. However, it is generally not true for the attachment processes, because a mother phase (vapor or liquid) consists of a mixture of *A, B*, and *C* atoms rather than III-V pairs. The atomic character of growth was earlier considered in Refs. [10,46] but not incorporated into the general kinetic scheme. Consequently, in this paper we develop a general approach for modeling the stationary composition of III-V ternary materials, which simultaneously accounts for the kinetics of the atomic growth and interactions of *AC* and *BC* pairs in a solid, which are determined by thermodynamic factors. We will show that the resulting vapor-solid distribution is a combination of the thermodynamic distribution given by Eq. (1) and the kinetic distribution given by Eq. (2), whose weights are determined primarily by the total flux ratio ε. At small $\varepsilon \ll 1$ the solid composition is controlled by the growth kinetics, as in Refs. [47–50]. At large $\varepsilon \gg 1$, the solid composition is driven by thermodynamics regardless of the supersaturation level in a mother phase. This growth is no longer controlled by supersaturation because, in the absence of available *C* atoms, *A* and *B* atoms accumulate near a growing interface and the growth conditions for them become close to thermodynamic equilibrium. We discuss the physical consequences of the obtained solution and fit the available data on the vapor-solid distributions of different III-V ternaries based on group V intermix.

II. METHOD

The method is based on the diffusion-induced growth model of Ref. [50], generalized to the case of arbitrary flux ratios of *A* and *B* over *C* atoms. We consider the vapor-solid growth of a ternary $A_xB_{1-x}C$ material in any geometry (epilayer, vapor-solid nanostructure, or VLS nanowire), described by the three stationary diffusion equations for the surface concentrations n_k [50]:

$$D_k \frac{d^2 n_k}{d\xi^2} + I_k - \frac{n_k}{\tau_k} = 0, \qquad k = A, B, C. \tag{3}$$

Here, ξ is the spatial coordinate; D_k are the surface diffusion coefficients of adatoms *A, B*, and *C*; I_k are the vapor fluxes of *A, B*, and *C* species; and τ_k are the desorption-limited lifetimes of adatoms. For group V atoms, Eq. (3) is valid only if the limiting step of the growth process is the reversible reaction of decomposition of a precursor containing one group V atom (for example, AsH_3, PH_3, or NH_3) in vapor phase epitaxy techniques such as metal-organic VPE (MOVPE) or hydride VPE (HVPE) with chloride precursors for group III species. In the case of deposition from dimers such as As_2, P_2, or N_2 and associative desorption in the form of dimers, as in MBE or in VPE where group V precursors decompose in the vapor phase before reaching the surface, one should use the flux of dimers $I_5 = 2I_5'$ (with I_5' as the atomic flux) and $\tau_5 = 1/(4\sigma_5 D_5 I_5)^{1/2}$, where σ_5 is the desorption probability of group V dimers. This corresponds to the effective diffusion length of group V adatoms $\lambda_5 = \sqrt{D_5\tau_5} = (D_5/4\sigma_5 I_5)^{1/4}$ and the spatially uniform concentration $n_5^0 = I_5\tau_5 = (I_5/4\sigma_5 D_5)^{1/2}$. Then, the linearized diffusion equation for group V adatoms with the average concentration n_5^0 has the same form as given by Eq. (3), where τ_5 and λ_5 depend on the vapor flux I_5 [50].

Equations (1) require six boundary conditions which should reflect the physics of the growth process. Introducing the spacing *P* which in the simplest case of epilayers depends on the distance between the growing steps, the diffusion fluxes should be zero between the steps by symmetry:

$$\left.\frac{dn_k}{d\xi}\right|_{\xi=P/2} = 0, \qquad k = A, B, C. \tag{4}$$

The two conditions at the boundary of a growing solid (at $\xi = 0$) are similar to Ref. [50], but generalized for spatially nonuniform surface concentration of *C* adatoms:

$$n_A(\xi = 0)n_C(\xi = 0) = (n_A n_C)^{\text{eq}} x e^{\omega(1-x)^2},$$
$$n_B(\xi = 0)n_C(\xi = 0) = (n_B n_C)^{\text{eq}}(1-x)e^{\omega x^2}. \tag{5}$$

Here, $(n_A n_C)^{\text{eq}}$ and $(n_B n_C)^{\text{eq}}$ are the equilibrium activities of *AC* and *BC* binaries and ω is the pseudobinary interaction constant. These boundary conditions are equivalent to the equality of the chemical potentials of *AC* and *BC* pairs in the perfect mixture of surface adatoms and in a ternary solid [10,11,39–45,47–50].

The remaining boundary condition should ensure the stoichiometry of an $A_xB_{1-x}C$ pseudobinary material [10,46]. The diffusion fluxes of *A, B*, and *C* atoms into a growing solid

material are determined by

$$j_k = D_k\left(\frac{dn_k}{d\xi}\right)_{\xi=0},$$
$$k = A, B, C. \tag{6}$$

Therefore, the sum of diffusion fluxes of A and B atoms should equal the diffusion flux of C atoms:

$$D_A\left(\frac{dn_A}{d\xi}\right)_{\xi=0} + D_B\left(\frac{dn_B}{d\xi}\right)_{\xi=0} = D_C\left(\frac{dn_C}{d\xi}\right)_{\xi=0}, \tag{7}$$

corresponding to $j_A + j_B = j_C$. Decoupling the binary fluxes of A and B atoms into the binary fluxes of AC and BC pairs, as in Refs. [47–50], would yield

$$D_A\left(\frac{dn_A}{d\xi}\right)_{\xi=0} = D_C\left(\frac{dn_C}{d\xi}\right)_{\xi=0},$$
$$D_B\left(\frac{dn_A}{d\xi}\right)_{\xi=0} = D_C\left(\frac{dn_C}{d\xi}\right)_{\xi=0}, \tag{8}$$

meaning that $j_A = j_C$ and $j_B = j_C$ separately. This is obviously wrong in the general case, and gives the nonphysical seventh boundary condition for the three second order diffusion equations. In Ref. [50], it was shown that decoupling of the binary fluxes is possible only under C-rich conditions (for example, group V rich conditions for an $A_xB_{1-x}C$ ternary based on group III intermix), where $n_c = n_c^0$ and hence the extra boundary condition given by Eq. (4) for n_c is not required.

In the following, we use the following definitions for the control parameters. The effective collection lengths are defined according to

$$\Lambda_k = \lambda_k \tanh\left(\frac{P}{2\lambda_k}\right), \tag{9}$$

$k = A, B, C$and can be adapted, for example, to describe different diffusivities of A, B, and C adatoms on the sidewalls of vertical nanowires [33,46,50]. If group V atoms impinge and desorb in the form of dimers, their effective diffusion length

$$\Lambda_5 = \left(\frac{D_5}{4\sigma_5 I_5}\right)^{1/4} \tanh\left[\frac{P}{(4D_5/\sigma_5 I_5)^{1/4}}\right] \tag{10}$$

depends on the vapor flux I_5 and becomes flux independent only at small P ($\Lambda_5 = P/2$). The effective incoming fluxes of A, B, and C atoms accounting for the collection lengths are given by

$$J_A = \Lambda_A I_A, \quad J_B = \Lambda_B I_B, \quad J_C = \Lambda_C I_C. \tag{11}$$

The functions describing the rejected fluxes are defined according to

$$F_A = \frac{\Lambda_A \Lambda_C}{\tau_A \tau_C}(n_A n_C)^{\mathrm{eq}} x e^{\omega(1-x)^2},$$
$$F_B = \frac{\Lambda_B \Lambda_C}{\tau_B \tau_C}(n_B n_C)^{\mathrm{eq}} (1-x) e^{\omega x^2}. \tag{12}$$

The composition of a ternary solid $A_xB_{1-x}C$ and the effective vapor composition are given by

$$x = \frac{j_A}{j_A + j_B} = \frac{j_A}{j_C}, \quad Z = \frac{J_A}{J_A + J_B}. \tag{13}$$

Clearly, Z becomes equal to the vapor composition z when the collections lengths of A and B adatoms are equal:

$$Z = z = \frac{I_A}{I_A + I_B} \text{ at } \Lambda_A = \Lambda_B, \tag{14}$$

regardless of Λ_C.

The three boundary conditions given by Eqs. (5) and (7) yield the following nonlinear system of algebraic equations for determination of the unknown j_A, j_B, and j_C:

$$j_A + j_B = j_C, \tag{15}$$

$$(J_A - j_A)(J_C - j_C) = F_A, \tag{16}$$

$$(J_B - j_B)(J_C - j_C) = F_B. \tag{17}$$

Nonlinearity of Eqs. (16) and (17) arises due to the nonlinear boundary conditions given by Eqs. (5), which contain the products of the two adatom concentrations. These expressions show that the actual diffusion fluxes into a growing ternary material j_k are smaller than the incoming fluxes J_k due to nonzero F_k, which describe the adatom fluxes rejected by a solid. Summations of Eqs. (16) and (17) together with Eq. (15) gives a quadratic equation for the total diffusion flux j_C:

$$j_c^2 - (J_A + J_B + J_C)j_C + (J_A + J_B)J_C - F_A - F_B = 0. \tag{18}$$

The solution has the form

$$\frac{j_C}{J_A + J_B} = G = \frac{1}{2}\frac{(1+\varepsilon)}{\varepsilon}\left[1 - \sqrt{1 - \frac{4\varepsilon\varphi}{(1+\varepsilon)^2}}\right]. \tag{19}$$

Here, the important parameter of our theory, which was absent in most kinetic models dealing with group C-rich growth [21,47–50], is given by

$$\varepsilon = \frac{J_A + J_B}{J_C}. \tag{20}$$

When all the collection lengths equal each other, this ε simply becomes the total III/V flux ratio (for ternaries based on group III intermix where A and B correspond to group III atoms) or V/III flux ratio (for ternaries based on group V intermix, where A and B correspond to group V atoms):

$$\varepsilon = \frac{I_A + I_B}{I_C} \text{ at } \Lambda_A = \Lambda_B = \Lambda_c = P/2. \tag{21}$$

The thermodynamic function φ is given by

$$\varphi = 1 - \frac{F_A + F_B}{J_C(J_A + J_B)}. \tag{22}$$

When ε is given by Eq. (21), and more generally when $\Lambda_A = \Lambda_B \neq \Lambda_C$, the function G defined by Eq. (19) depends on the flux ratio and solid composition x present in φ, but is independent of the vapor composition z. The function φ depends, however, on the product of the total group III and V fluxes $I_C(I_A + I_B)$. When $\Lambda_A \neq \Lambda_B$, as usual for group III adatoms A and B, the situation becomes more complex because Z, ε, and φ depend on the vapor composition z.

Dividing Eq. (16) by Eq. (17) and using again Eq. (15) allows one to obtain explicitly the effective vapor-solid distribution in the form

$$Z = \frac{1}{1 + F_B/F_A}(1 - G) + xG. \tag{23}$$

Using Eqs. (12), the ratio F_B/F_A entering this solution can be presented as $F_B/F_A = f(x)/c$, where $f(x)$ is the thermodynamic function defined in Eq. (1) and

$$c = \frac{\Lambda_A}{\Lambda_B} \tag{24}$$

is the kinetic constant accounting for the possible difference in the collection lengths for A and B adatoms. Hence, Eq. (23) can equivalently be presented as

$$Z = \frac{1}{1 + f(x)/c}(1 - G) + xG, \tag{25}$$

which is the main result of this paper. This exact solution for the vapor-solid distribution applies at arbitrary fluxes or flux ratios, with the functions $1/[1 + f(x)/c]$ and x corresponding to the thermodynamic and kinetic limits as will be discussed shortly. When $\Lambda_A = \Lambda_B$, $Z = z$ is the vapor composition and the function G in the right-hand side of Eq. (25) is independent of z, which provides the explicit form of the $z(x)$ dependence in this case. When $\Lambda_A \neq \Lambda_B$, Eq. (25) provides the vapor-solid distribution $z(x)$ only implicitly. However, the explicit form of $z(x)$ can be resumed in some important particular cases discussed in the next section.

III. RESULTS AND DISCUSSION

A. Equilibrium solution

The equilibrium solution in our model corresponds to $\varphi = 0$, which yields $G = 0$ according to Eq. (19). Using Eqs. (22), (11), and (12), the function φ can be presented as

$$\varphi = 1 - \frac{1}{cz + 1 - z}\Gamma[cxe^{\omega(1-x)^2} + \beta_0(1 - x)e^{\omega x^2}], \tag{26}$$

where z is the actual vapor composition and Γ is the parameter entering the kinetic vapor-solid distribution given by Eq. (2). The equilibrium condition $\varphi = 0$ requires that the total diffusion flux $j_C = j_A + j_B = 0$. However, from Eqs. (16) and (17) it follows that $j_A = 0$ and $j_B = 0$ separately, which corresponds to the total equilibrium with zero diffusion fluxes of A, B, and C adatoms. Using the known expressions for the chemical potentials μ_{AC} and μ_{BC} of AC and BC pairs in a solid [41,45], and the chemical potentials μ_A, μ_B, and μ_C of A, B, and C atoms in the perfect gas of adatoms surrounding a ternary solid, Eqs. (26), (16), and (17) yield

$$\begin{aligned} \mu_A + \mu_C &= \mu_{AC}, \\ \mu_B + \mu_C &= \mu_{BC}. \end{aligned} \tag{27}$$

This corresponds to the two equilibria for AC and BC pairs in a mother phase and solid, as in Refs. [32,41], which are equivalent to the condition $j_A = j_B = j_C = 0$ in our model.

From Eq. (25), $Z = 1/[1 + f(x)/c]$ under equilibrium conditions. Using the definition for Z given by Eqs. (13) and (11) for J_A and J_B, we find

$$Z = \frac{cz}{cz + 1 - z}. \tag{28}$$

Comparing these two results for Z, the vapor-solid distribution under equilibrium conditions is given by Eq. (1), i.e., by the two-parametric thermodynamic formula. It is interesting to note that the general equilibrium condition $\varphi = 0$ contains the vapor flux of C atoms and the kinetic constant c, which cancel in the resulting thermodynamic vapor-solid distribution.

B. Interplay of kinetics and thermodynamics

From Eq. (19), the function G is bound in the range from $\varphi/(1 + \varepsilon)$ at $\varepsilon \gg 1$ to φ at $\varepsilon \ll 1$, while φ itself is less than unity in the growth conditions, with $\varphi = 0$ corresponding to the no-growth conditions at equilibrium. Another limiting case of $\varphi = 1$ corresponds to growth at very high supersaturations [$\Gamma \to 0$ in Eq. (26)]. Therefore, we have

$$0 \leqslant \frac{\varphi}{1 + \varepsilon} \leqslant G \leqslant \varphi \leqslant 1, \tag{29}$$

showing that G changes from zero at $\varphi = 0$ or $\varepsilon \to \infty$ regardless of φ to unity at $\varepsilon \to 0$ and $\varphi = 1$. From these considerations, $1-G$ can be treated as the probability for realization of the equilibrium state and G can be treated as the probability for realization of the kinetic state for A and B atoms whose intermix forms a ternary solid. Importantly, $G = G(\varepsilon)$ depends on the flux ratio ε. At small $\varepsilon \ll 1$, $G = \varphi$ and hence the weights of the thermodynamic and kinetic distributions equal $1-\varphi$ and φ, respectively. Under strongly nonequilibrium growth conditions corresponding to $\varphi \ll 1$, the solid composition is kinetically driven, as discussed, for example, in Refs. [21,48,50]. This corresponds to $Z = x$ according to Eq. (25), with no thermodynamic factors left in the vapor-solid distribution. Conversely, at large $\varepsilon \gg 1$ the weight of the growth kinetics tends to zero and the vapor-solid distribution becomes equilibrium. This is explained by the fact that only a small fraction of the arriving A and B atoms are incorporated into a solid due to the lack of available C atoms in a mother phase. In this regime, the state of the mother phase becomes very close to equilibrium for A and B atoms, regardless of their vapor fluxes.

Figure 1 shows the vapor-solid distribution given by Eq. (25) at $\Lambda_A = \Lambda_B$ (corresponding to $c = 1$) for the fixed thermodynamic parameters $\omega = 2.3$ and $\beta_0 = 0.1$ at different ε from 0.1 to 10, compared to the kinetic distribution given by Eq. (2) at $\varepsilon \to 0$. We assume that ε is raised by increasing the vapor fluxes of A and B atoms rather than decreasing the vapor flux of C atoms. In this case, the parameter Γ in Eq. (2) is inversely proportional to ε. The starting curve at $\varepsilon = 0.1$ and $\Gamma = 0.3$ is indistinguishable from the distribution at $\varepsilon \to 0$, confirming the validity of the models of Refs. [47–50] in the C-rich growth regime. Increasing the vapor supersaturations by fluxes I_A and I_B decreases the contribution of the Γ term in Eq. (26) and increases the value of φ toward unity. This leads to a more linear kinetically controlled curve at $\varepsilon = 0.3$, which remains very close to the curve given by Eq. (2). However, at $\varepsilon = 1$ the difference between the general vapor-solid distribution and its approximation by Eq. (2) at $\varepsilon \to 0$ becomes significant. The actual distribution becomes more nonlinear than at $\varepsilon = 0.3$, while the curve at $\varepsilon \to 0$ wrongly predicts the purely kinetic regime with the linear correlation $z = x$, which does not change with further increase of ε. The general distribution becomes more and more nonlinear as ε increases from 0.3 to 10, and tends to the equilibrium curve at $\varepsilon \to \infty$. Therefore, thermodynamically controlled

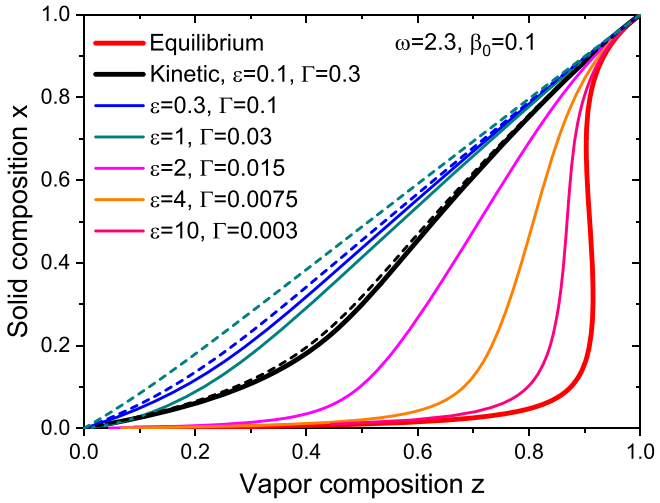

FIG. 1. General vapor-solid distribution at a fixed $c = 1$, $\omega = 2.3$, and $\beta_0 = 0.1$ for different ε and Γ shown in the legend (solid lines), compared to the kinetic distribution at $\varepsilon \to 0$ given by Eq. (2) (dashed lines). It is assumed that the increase of ε is achieved by increasing vapor fluxes of A and B atoms, in which case Γ in Eq. (2) scales as $1/\varepsilon$. The bold red line shows the equilibrium distribution given by Eq. (1), which contains the miscibility gap. The general vapor-solid distribution is close to the kinetic curves only at small $\varepsilon \leqslant 0.3$. Further increase of ε renders the solid composition into the close-to-equilibrium conditions despite very high supersaturation at $\Gamma \to 0$.

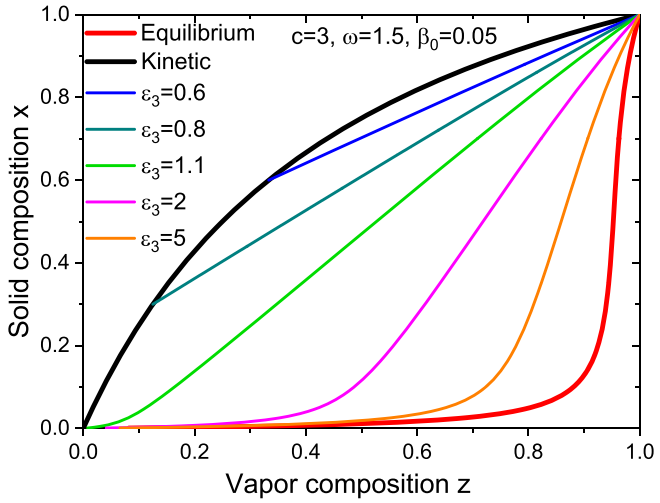

FIG. 2. Vapor-solid distributions for a III-V ternary based on group III intermix at infinitely high vapor supersaturation ($\varphi \to 1$), obtained from Eq. (32) at a fixed $c = 3$, $\omega = 1.5$, $\beta_0 = 0.05$ and different effective III/V flux ratios ε_3 shown in the legend. The red bold line shows the equilibrium distribution. The black bold line shows the purely kinetic distribution which favors the incorporation of A adatoms due to their larger collection length compared to B adatoms, and pertains to all $\varepsilon_3 \leqslant 0.5$. Further increase of the III/V flux ratio modifies the kinetic curve first at large x and then in the entire range of compositions. At large $\varepsilon_3 \gg 1$ the vapor-solid distribution acquires the equilibrium shape despite infinitely high vapor supersaturation.

composition of ternary III-V materials is observed not only under no-growth conditions (at $\varphi \to 0$), but also during C-poor growth regardless of φ and even under infinitely high supersaturation (at $\varphi \to 1$). The model assuming C limited growth works well at small enough ε but is totally wrong at large $\varepsilon > 1$. This is not surprising, because this model is valid only at $\varepsilon \ll 1$ and should not be used under C poor conditions. When $c \neq 1$, the purely kinetic distribution is given by the nonlinear Langmuir-McLean equation [51]. The intermediate regimes become more complex due to the z-dependent Z and ε, as will be discussed shortly.

C. Growth at high supersaturations

Growth under very high supersaturations often occurs for ternaries based on group III intermix in the regimes without desorption of group III atoms from a substrate surface or nanowire sidewalls and catalyst droplets at a growth temperature [32,33,39], and may occur for ternaries based on group V intermix at low temperatures [39,46]. This corresponds to $\varphi \to 1$ in Eq. (19) for G, yielding $G = 1$ at $\varepsilon \leqslant 1$ and $G = 1/\varepsilon$ at $\varepsilon > 1$. Equation (25) is then reduced to

$$Z = \begin{cases} x \text{ at } \varepsilon \leqslant 1 \\ \frac{1}{1+f(x)/c}\left(1 - \frac{1}{\varepsilon}\right) + \frac{x}{\varepsilon} \text{ at } \varepsilon > 1 \end{cases}. \tag{30}$$

This expression can be used directly for ternaries based on group V intermix at $\Lambda_A = \Lambda_B$ and a z-independent β_0, which corresponds to "atomic" flux of group V precursors rather than a flux of V_2 dimers. In this case, we simply have $Z = z$, and $\varepsilon = (\Lambda_5/\Lambda_3)[(I_A + I_B)/I_3]$ as the effective V/III flux ratio, with $\Lambda_3 = \Lambda_B$ and $\Lambda_5 = \Lambda_C$.

For ternaries based on group III intermix, for which $\Lambda_A \neq \Lambda_B$ in the general case, we have

$$\varepsilon = \varepsilon_3(cz + 1 - z),$$
$$\varepsilon_3 = \frac{\Lambda_3}{\Lambda_5}\frac{(I_A + I_B)}{I_5}, \tag{31}$$

whereas Z is related to the vapor composition z by Eq. (28). From Eq. (30), it is easy to obtain the explicit form of the vapor-solid distribution in the form of $z(x)$ dependence:

$$z = \frac{x}{c + (1-c)x},$$
$$z \leqslant \frac{1/\varepsilon_3 - 1}{c - 1},$$
$$z = \frac{1}{1+f(x)}\left(1 - \frac{1}{\varepsilon_3}\right) + \left(\frac{1+f(x)/c}{1+f(x)}\right)\frac{x}{\varepsilon_3},$$
$$z > \frac{1/\varepsilon_3 - 1}{c - 1}, \tag{32}$$

where we choose an element with a larger collection length as an A element in an $A_xB_{1-x}C$ ternary ($\Lambda_A > \Lambda_B$), corresponding to $c > 1$. Figure 2 shows the evolution of the vapor-solid distribution from the purely kinetic shape at low III/V flux ratios $\varepsilon_3 \leqslant 0.5$ to the equilibrium shape at large $\varepsilon_3 \gg 1$. The equilibrium state at large ε_3 is achieved under group III

rich growth conditions at infinitely high supersaturation of a mother phase, like in Fig. 1.

It should be noted that ε_3 given by Eq. (31) contains the ratio of collection lengths of group III over group V adatoms, Λ_3/Λ_5. This ratio equals unity for epilayers with high density of steps, but is larger or even much larger than unity for VLS III-V nanowires, where the surface diffusivity of group III adatoms on the nanowire sidewalls is larger (typically on the order of 100–1000 nm) compared to group V adatoms [33,39,46,50]. Of course, the vapor-solid distribution at large enough ε_3 becomes liquid-solid due to a group III liquid (in liquid phase epitaxy) or an Au-*A*-*B*-*C* alloy (in VLS nanowires) surrounding a growing island. These considerations show that the purely kinetic growth of VLS ternary nanowires based on group III intermix rarely occurs under group V rich conditions and hence the model at $\varepsilon \to 0$ based on Eq. (2) (for the liquid-solid distributions [47,49]) has a limited range of applications for these nanomaterials. However, it works well for vapor-solid InGaN nanowires grown under very low III/V ratios [21], and may be relevant for the vapor-solid distributions of VLS InGaAs nanowires [26,29,31,50] at low desorption rates of In atoms, with the miscibility gaps suppressed in both systems.

For ternaries based on group V intermix deposited from the vapor fluxes of V_2 dimers such as As_2 or P_2, one can assume $\Lambda_A = \Lambda_B$ and hence $Z = z$. However, the compositional diagram is complicated by a z-dependent β_0 in Eq. (1) due to the flux-dependent effective desorption times for A and B adatoms. In this case, we have

$$\beta_0 = \beta_5\left(\frac{1-z}{z}\right)^{1/2},$$
$$\beta_5 = \left(\frac{\sigma_B D_B}{\sigma_A D_A}\right)^{1/2}\frac{(n_B n_C)^{\rm eq}}{(n_A n_C)^{\rm eq}},$$
$$\varepsilon = \varepsilon_5 = \frac{\Lambda_5}{\Lambda_3}\frac{(I_A + I_B)}{I_3}. \tag{33}$$

From Eq. (30), the vapor-solid distribution takes the form

$$z = x,\ \varepsilon_5 \leqslant 1,$$
$$z = \frac{1}{1 + f(x)\left(\frac{1-z}{z}\right)^{1/2}}\left(1 - \frac{1}{\varepsilon_5}\right) + \frac{x}{\varepsilon_5},$$
$$\varepsilon_5 > 1,$$
$$f(x) = \beta_5\frac{(1-x)}{x}e^{\omega(2x-1)}. \tag{34}$$

At $\varepsilon_5 > 1$, this yields a cubic equation for $t = [(1-z)/z]^{1/2}$, which can be presented in the form

$$\frac{1}{1+t^2} = \frac{1}{1+f(x)t}\left(1 - \frac{1}{\varepsilon_5}\right) + \frac{x}{\varepsilon_5}. \tag{35}$$

It is clear that $z = 1/(1+t^2) \cong x/\varepsilon_5$ when ε_5 is close to 1, and $t \cong f(x)$ at $\varepsilon_5 \gg 1$. Therefore, the approximate solution for the vapor-solid distribution can be presented in the form

$$z = \frac{1}{1+f^2(x)}\left(1 - \frac{1}{\varepsilon_5}\right) + \frac{x}{\varepsilon_5}. \tag{36}$$

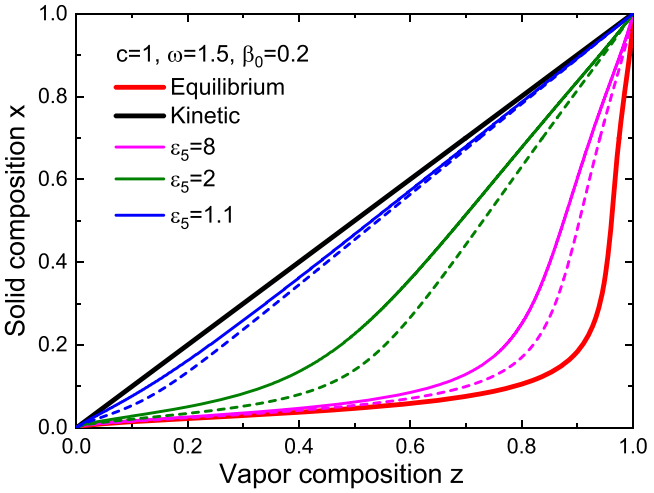

FIG. 3. Vapor-solid distributions for a III-V ternary based on group V intermix at infinitely high supersaturation ($\varphi \to 1$), obtained from Eq. (34) (solid lines) and Eq. (36) (dashed lines) at a fixed $c = 1$, $\omega = 1.5$, $\beta_0 = 0.2$ and different effective V/III flux ratios ε_5 shown in the legend. The distribution evolves from the thermodynamically controlled shape at $\varepsilon_5 = 8$ to an almost linear kinetic shape at $\varepsilon_5 = 1.1$. The bold red line shows the equilibrium distribution, and the black bold line shows the linear kinetic distribution $z = x$, which is observed for any $\varepsilon_5 \leqslant 1$.

This solution is a linear combination of the equilibrium distribution at large effective V/III flux ratios (which is similar to the result of Ref. [11] for As_4 and Sb_4 growth species forming InSbAs epilayers), which prevails at $\varepsilon_5 \gg 1$, and the kinetic distribution, which prevails at $\varepsilon_5 \ll 1$. Figure 3 shows the evolution of the vapor-solid distribution from the equilibrium to kinetic shape with the decrease of the effective V/III flux ratio and demonstrates that Eq. (36) provides a reasonable approximation to the exact solution for all ε_5.

According to Eq. (33), the effective V/III flux ratio ε_5 contains the ratio of the collection lengths Λ_5/Λ_3, which is on the order of unity for epilayers but much less than unity for nanowires. The vapor-solid growth of ternary epilayers or nanowires should occur under group V rich conditions to avoid the formation of a group III liquid, which corresponds to $\varepsilon_5 \geqslant 1$ or even $\varepsilon_5 \gg 1$ [10]. The same applies for catalyst-free III-V ternary nanowires grown in the vapor-solid mode [23–25]. The vapor-solid distributions of the vapor-solid ternaries based on group V intermix grown under group V rich conditions are expected to be close to equilibrium, as indeed observed, for example, for $InSb_xAs_{1-x}$ epilayers of Refs. [10,11], $AlSb_xAs_{1-x}$ of Ref. [12], and vapor-solid $InSb_xAs_{1-x}$ nanowires of Ref. [23]. Close-to-linear kinetic curves in different vapor-solid $III-V_xV_{1-x}$ materials require that $\varepsilon_5 \cong 1$ [9,10,12]. In VLS nanowires, the values of ε_5 are strongly decreased relative to their nominal values in vapor by surface diffusion of group III adatoms to the droplets, as noted previously in Ref. [35] for Au-catalyzed VLS $InSb_xAs_{1-x}$ nanowires. Consequently, close-to-linear kinetic shapes of the liquid-solid or vapor-solid [35,53–55] distributions of VLS $III-V_xV_{1-x}$ nanowires should be more easily achieved compared to epilayers or vapor-solid nanostructures and nanowires. This conclusion will be further elaborated in the next section.

D. Linearized model for ternaries based on group III intermix

Equation (19) for G can be linearized at

$$\frac{4\varepsilon\varphi}{(1+\varepsilon)^2} \ll 1, \tag{37}$$

which is valid for any ε at $\varphi \ll 1$, and for any φ at $\varepsilon \ll 1$ or $\varepsilon \gg 1$. The function G in the general distribution given by Eq. (25) can then be approximated as $G = \varphi/(1+\varepsilon)$. Using Eq. (26) for φ and considering ternaries based on group III intermix, the vapor-solid distribution can be obtained in the analytic form (below we again assume that $c > 1$):

$$\begin{aligned} z(x) &= \frac{t(x)-1}{c-1}, \\ t(x) &= \begin{matrix} \frac{Y(x)}{2}[1-\sqrt{1+4Z(x)}], & Y \leqslant 0 \\ \frac{Y(x)}{2}[1+\sqrt{1+4Z(x)}], & Y > 0 \end{matrix}, \\ Y(x) &= \frac{1+f(x)/c}{1+f(x)}\frac{(c-1)x+c(\varepsilon_3-1)}{\varepsilon_3}, \\ Z(x) &= \varepsilon_3\frac{1+f(x)}{1+f(x)/c}\frac{(c-1)g(x)+c}{[(c-1)x+c(\varepsilon_3-1)]^2}, \end{aligned} \tag{38}$$

with the kinetic function $g(x)$ given by

$$g(x) = (1-x)x\Gamma[ce^{\omega(1-x)^2} - \beta_0 e^{\omega x^2}]. \tag{39}$$

Here, the effective III/V flux ratio ε_3 is the same as in Eq. (31).

This solution is reduced to the equilibrium distribution at $\varepsilon_3 \gg 1$, while at $\varepsilon_3 \ll 1$ it yields the result of Ref. [50] given by Eq. (2):

$$z = \frac{x+g(x)}{c+(1-c)x}. \tag{40}$$

Therefore, the obtained vapor-solid distribution is a nonlinear combination of the equilibrium and kinetic distributions given by Eqs. (1) and (2), respectively. The nonlinearity arises due to $\Lambda_A \neq \Lambda_B$, which leads to z-dependent $Z(z)$ and $\varepsilon(z)$ according to Eqs. (28) and (31). The linearized model becomes exact at $\varepsilon_3 \ll 1$ and $\varepsilon_3 \gg 1$ regardless of φ, while for ε_3 around unity its accuracy is guaranteed only at small enough φ corresponding to the growth at low supersaturations. This property is demonstrated in Fig. 4 which shows a comparison of numerical solution to Eq. (25) with G given by Eq. (19) to the approximation given by Eq. (38) with the linearized $G = \varphi/(1+\varepsilon)$. As expected, the approximate solution is perfect at $\varepsilon_3 = 0.2$ and 5, but becomes inaccurate at $\varepsilon_3 = 1$ for these parameters.

Our analysis shows that the analytic compositional diagrams $x(z)$ can only be obtained in the four cases considered above. However, these solutions should be sufficient for the full description of the vapor-solid distributions in a wide range of growth conditions. Indeed, III-V ternary materials based on group III intermix are fully described by Eq. (38) under group V rich and group V poor conditions, while the growth at high supersaturations is well described by Eq. (32) at $\varphi = 1$. The general Eq. (25) at $Z = z$ is directly applicable for the reaction-limited growth of III-V ternaries based on group V intermix from precursors containing one group V atom. Equation (34) or its approximation given by Eq. (36) fully describes the composition of III-V ternaries based on group V intermix grown from V_2 dimers at high supersaturations, and only growth at moderate supersaturations may require numerical solution of the general Eq. (25).

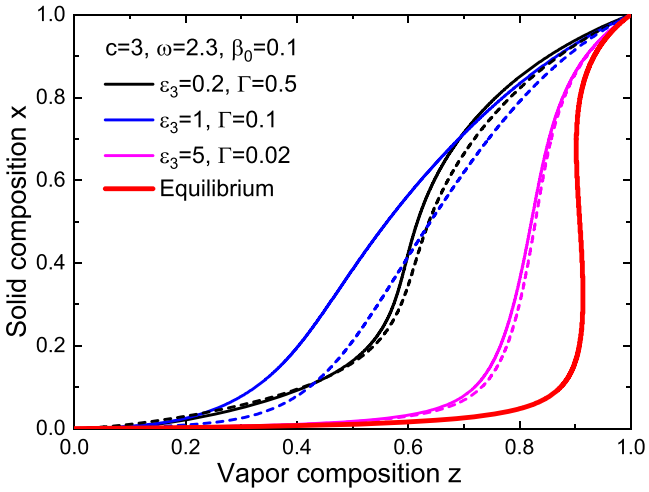

FIG. 4. Vapor-solid distributions for a III-V ternary based on group III intermix at a fixed $c = 3$, $\omega = 2.3$, $\beta_0 = 0.1$ and different ε_3 shown in the legend, obtained numerically from G in Eq. (25) given by Eq. (19) (solid lines), and from the approximate analytical solution given by Eq. (38) with $G = \varphi/(1+\varepsilon)$ (dashed lines). As in Fig. 2, we assume that the increase of ε_3 is achieved by increasing A and B vapor fluxes, in which case Γ scales as $1/\varepsilon$. The red bold line shows the equilibrium distribution containing the miscibility gap.

IV. THEORY AND EXPERIMENT

In this section, we consider the available data on the vapor-solid distributions of III-V ternary epilayers and VLS nanowires based on group V intermix, which depend on the total V/III flux ratio. Refined modeling of III-V ternary materials and nanomaterials based on group III intermix, including VLS nanowires, will be presented elsewhere. $InSb_xAs_{1-x}$ epilayers of Ref. [10] were grown by MOVPE using trimethylindium (TMIn), trimethylantimony (TMSb), and AsH_3 precursors, at a temperature of 475 °C. The total V/III flux ratios were varied in a wide range by tuning the partial pressures of group V precursors, which did not affect the In-limited total growth rate. Pyrolysis of group V precursors at the surface produced As_4 and Sb_4 vapors according to the surface reactions originally considered in Ref. [10]. We will use, however, the model involving As_2 and Sb_2 dimers rather than tetramers according to the general view based on the fact that the equilibrium pressures of V_2 vapors are much larger compared to V_4 vapors [56,57] and that group V elements always desorb in the form of dimers [57]. $InSb_xAs_{1-x}$ epilayers of Ref. [11] were grown by MOVPE using triethylindium (TEIn), triethylantimony (TESb), and AsH_3 precursors, at a temperature of 500 °C. The total III/V flux ratio was more than 15, as estimated from the ratio of partial pressures of TESb and TEIn given in Ref. [11].

Figure 5 shows the vapor-solid distributions of $InSb_xAs_{1-x}$ epilayers obtained in Refs. [10,11] and their fits by Eq. (36) with the parameters given in Table I. Equation (36) contains a minimum number of parameters which include the total

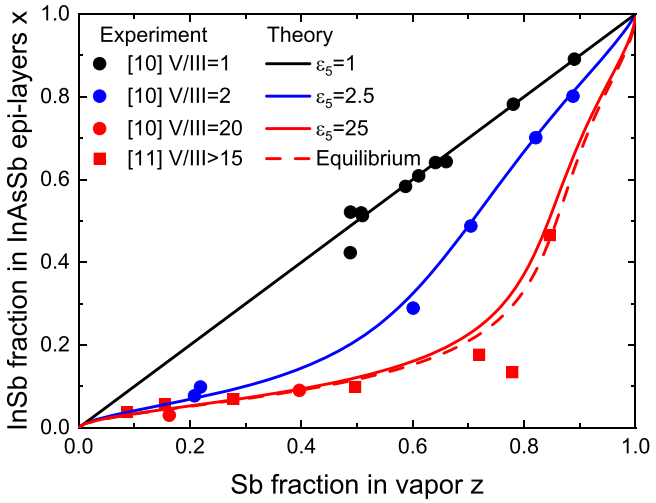

FIG. 5. Vapor-solid distributions of $InSb_xAs_{1-x}$ epilayers of Refs. [10] (circles) and [11] (squares) grown by MOVPE under different total V/III flux ratios, fitted by the model with the ε_5 values shown in the legend and other parameters summarized in Table I (lines). The distributions change from the linear kinetic shape at a V/III flux ratio of 1 to the nonlinear equilibrium shape (the dashed line) at large V/III flux ratios, as predicted by the model.

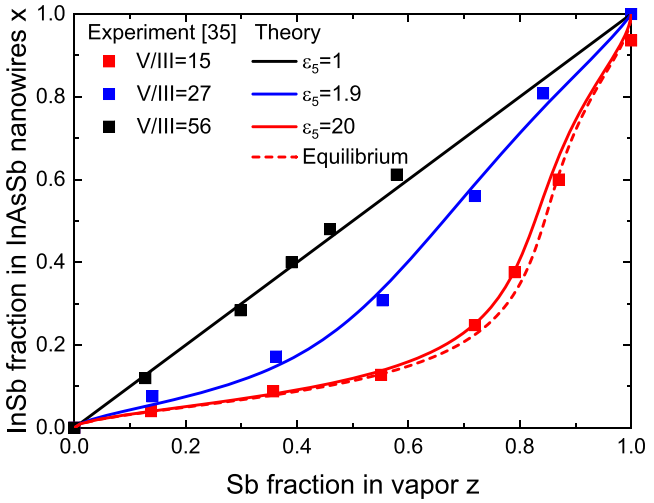

FIG. 6. Vapor-solid distributions of Au-catalyzed VLS $InSb_xAs_{1-x}$ nanowires of Refs. [35], grown by MOVPE under different total V/III ratios shown in the legend (symbols), fitted by the model with the ε_5 values shown in the legend and other parameters summarized in Table I (solid lines). The dashed line shows the equilibrium distribution. As in Fig. 5, the distributions change from the linear kinetic curve at the lowest V/III ratio to the equilibrium shape at the highest V/III ratio. The fitting values of ε_5 shown in the legend are significantly lower than the V/III flux ratios in the vapor phase due to the additional diffusion flux of In adatoms from the nanowire sidewalls to the catalyst droplets.

V/III flux ratio ε_5 and the thermodynamic constants ω and β_0 in the equilibrium distribution given by Eq. (1). We used a composition-independent InAs-InSb pseudobinary interaction parameter of 2250 cal/mol given in Ref. [1], which yields the values of ω given in Table I. For $\beta_0 = K_{InSb}/K_{InAs}$, where K_{InSb} and K_{InAs} are the equilibrium constants of surface reactions producing InSb and InAs pairs, respectively, we used a value of 2.33 at 475 °C [10] and 2.46 at 500 °C [11]. It is seen that our simple analytical expression provides good fits to the data and describes very well the observed transition from the kinetically controlled to the thermodynamically limited vapor-solid distribution with increasing the total V/III flux ratio. The values of ε_5 obtained from the best fits, shown in the legend and listed in Table I, appear close to the experimentally reported values [10]. The curve at $\varepsilon_5 = 25$ is very close to the equilibrium distribution, which also provides a good fit to the data of Ref. [11]. Using the general model does not significantly improve the fits. In Ref. [10], the compositional data were fitted by the original model which required numerical solution of the four equations for chemical reactions in vapor and at the growth interface, while the data of Ref. [11] were fitted by the equilibrium distribution for As_4 and Sb_4 tetramers. Our Eq. (36) contains both models and provides a simple analytical expression describing the observed interplay between the kinetic and thermodynamic factors depending on the total V/III ratio.

TABLE I. Parameters of $InSb_xAs_{1-x}$ and $AlSb_xAs_{1-x}$ materials.

Material	T (°C)	V/III ratios	ε_5	ω	β_0
$InSb_xAs_{1-x}$ epilayers [10]	475	1–20	1–25	1.514	2.33
$InSb_xAs_{1-x}$ epilayers [11]	500	>15	25	1.465	2.46
$InSb_xAs_{1-x}$ nanowires [35]	450	15–56	1–20	1.566	3.358
$AlSb_xAs_{1-x}$ epilayers [12]	600	1–4.4	1–4.4	2.215	3.358

Au-catalyzed VLS $InSb_xAs_{1-x}$ nanowires of Ref. [35] were grown by MOVPE using TMIn, TMSb, and AsH_3 precursors, with 50-nm-diameter colloidal Au nanoparticles as the nanowire growth seeds, at a temperature of 450 °C. The total V/III flux ratio was varied from 15 to 56 by varying group V molar fractions at a constant TNIn molar fraction. Figure 6 shows the data and their fits by Eq. (36) with the ε_5 values shown in the legend and other parameters summarized in Table I. For β_0, we used a value of 3.358 at 450 °C given in Ref. [35], and the same InSb-InAs pseudobinary interaction parameter of 2250 cal/mol as before. In contrast to epilayers, the fitting values of ε_5 appear significantly lower than the actual V/III ratios in the vapor phase. This effect was noticed in the original work [35], where the fits to the data by the model of Biefeld [10] required much lower V/III ratios than their nominal values in vapor. As discussed above, In adatoms have a much larger diffusivity on the nanowire sidewalls than group V adatoms, which gives an additional flux of In into the droplet and reduces the effective V/III flux ratios with respect to the vapor phase.

$AlSb_xAs_{1-x}$ epilayers of Ref. [12] were grown by MOVPE using TMAl, TMSb, and AsH_3 precursors, at a temperature of 600 °C. The total V/III flux ratios were varied from 1 to 4.4 by increasing the partial pressures of group V precursors. Figure 6 shows the measured vapor-solid distributions, fitted by Eq. (36) with the ε_5 values corresponding exactly to the V/III flux ratios in the vapor phase, and other parameters given in Table I. We used a value of 3.358 for $\beta_0 = K_{AlSb}/K_{AlAs}$

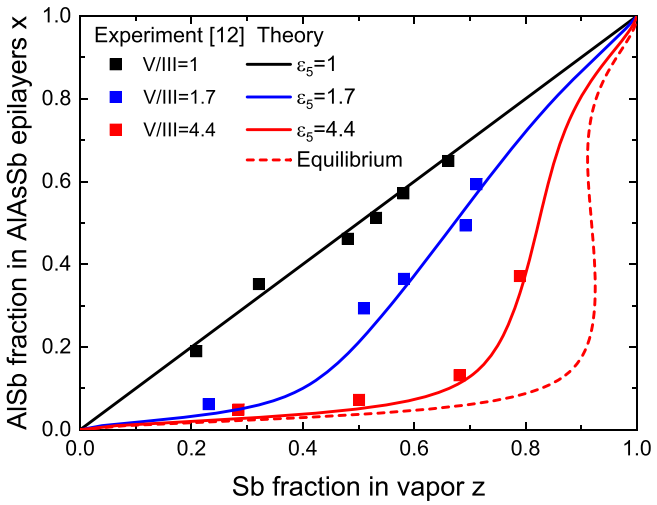

FIG. 7. Vapor-solid distributions of $AlSb_xAs_{1-x}$ epilayers of Refs. [12] (symbols), fitted by Eq. (36) (solid lines) with $\varepsilon_5 =$ V/III and other parameters given in Table I. The dashed line shows the equilibrium distribution with the miscibility gap, which is not reached at $\varepsilon_5 = 4.4$. However, the trend for changing the solid composition from the kinetically controlled to the thermodynamically limited shape at larger ε_5 is clear and very similar to Figs. 5 and 6.

at 600 °C and a value of 3843 cal/mol for the AlSb-AlAs pseudobinary interaction parameter, given in the original work [12]. The corresponding value of ω of 2.215 is larger than 2, which yields the miscibility gap in the equilibrium vapor-solid distribution shown in Fig. 6. This state is not reached at the highest V/III flux ratio of 4.4 employed in Ref. [12], but the evolution of the vapor-solid distribution from the kinetic to equilibrium shape with increasing ε_5 is clear. Overall, all the vapor-solid distributions shown in Figs. 5–7 feature exactly the same compositional trend for changing the solid composition from the kinetically controlled to the thermodynamically limited regime by increasing the total V/III ratio. We suspect that this effect is general and will pertain for any material system and nanostructure geometry, as predicted by our model.

V. CONCLUSIONS AND OUTLOOK

In summary, we have developed a general model for the diffusion-induced growth of III-V ternary materials and nanostructures. The model is based on the three coupled diffusion equations for *A, B*, and *C* adatoms with the appropriate boundary conditions. Most importantly, we have used the boundary condition for the diffusion fluxes in the form $j_A + j_B = j_C$ beyond the approximation of binary fluxes of *AC* and *BC* pairs entering a ternary solid. This enables treatment of the vapor-solid distributions of $A_xB_{1-x}C$ ternaries based on group III or group V intermix at arbitrary flux ratios. It has been shown that the general vapor-solid distribution is given by a combination of the kinetic and equilibrium distribution, whose probability depends on the total flux ratio of *A*+*B* over *C* atoms ε. The kinetically controlled regime occurs at $\varepsilon \ll 1$, where the growth is controlled by the attachment of *A* and *B* atoms in the excess of *C* atoms. This was a usual assumption in most kinetic models developed so far. In the opposite case of $\varepsilon \gg 1$, *A* and *B* atoms are accumulated in a mother phase and the growth conditions become close to equilibrium for them. Therefore, the vapor-solid distribution becomes thermodynamically controlled, even if the supersaturation level in a mother phase is infinitely high. As a result, our approach provides a general tool for modeling the vapor-solid distributions under arbitrary material fluxes and describes the interplay between the kinetic and thermodynamic factors depending on the total flux ratio. In most important cases, our model is reduced to simple analytical expressions with a minimum number of parameters, which are convenient for analyzing the compositional data. We have fitted the measured compositions of $InSb_xAs_{1-x}$ and $AlSb_xAs_{1-x}$ epilayers and Au-catalyzed VLS $InSb_xAs_{1-x}$ nanowires grown under different total V/III flux ratios by the same equation containing only the known thermodynamic parameters ω and β_0 and the V/III flux ratio ε_5. In all cases, the vapor-solid distributions converged from the linear kinetic shape at $\varepsilon_5 = 1$ to the nonlinear close-to-equilibrium shape at $\varepsilon_5 \gg 1$. This effect should have a general character and pertain for any III-V ternary. Furthermore, our model should work equally well for any stoichiometric ternary material.

Our analysis shows that the kinetic suppression of the miscibility gaps in highly mismatched III-V ternary systems such as InGaAs, InGaN, or AlSbAs requires growth at low ε rather than at high supersaturations of a mother phase. More generally, the kinetically controlled composition of an $A_xB_{1-x}C$ ternary requires that its growth is limited by *A* and *B* atoms whose intermix produces this ternary. Such conditions are typical for the vapor-solid growth of ternaries based on group III intermix at high enough V/III flux ratios, and for all VLS growths of ternary nanowires based on group V intermix. The linear shape of the vapor-solid distributions for the vapor-solid ternaries based on group V intermix is observed only at $\varepsilon_5 \cong 1$, as supported by the data on InSbAs and AlSbAs epilayers. Larger V/III flux ratios yield nonlinear shapes of the distributions. The vapor-solid growth of ternaries based on group III intermix at V/III flux ratios around unity should be considered using the general scheme, where the ε-dependent corrections become important. The VLS growth of III-V ternary nanowires based on group III intermix should proceed under close-to-equilibrium conditions for group III atoms in a catalyst droplet. This conclusion was used (indirectly and without explanation), for example, in Ref. [32], where the liquid-solid distribution of self-catalyzed VLS $Al_xGa_{1-x}As$ nanowires was taken in the equilibrium form and worked well for modeling the interfacial profiles across GaAs/AlGaAs nanowire heterostructures, and in Refs. [42–45], where the liquid-solid distributions of VLS ternary nanowires based on group III intermix were assumed nucleation limited. The existing kinetic models for the liquid-solid distributions of VLS ternary nanowires based on group III intermix [47,49] are based on the assumption $\varepsilon_3 \ll 1$ and therefore require a refinement from the viewpoint of the obtained results. We believe that the liquid-solid distributions of such nanowires should be close to equilibrium. In our analysis, we have not introduced directly a liquid phase of the droplet on the nanowire top and have not considered a nontrivial correlation between the liquid-solid

growth of nanowire monolayers and the vapor-liquid material exchange feeding the droplet from vapor. For example, in the absence of desorption of group III atoms from a catalyst droplet and nanowire sidewalls, the vapor-solid distribution of ternary III-V nanowires based on group III intermix should be given by the purely kinetic Langmuir-McLean formula [33,50], while the liquid-solid distribution should be close to equilibrium. We plan to consider this important question in a forthcoming work.

ACKNOWLEDGMENT

V.G.D. gratefully acknowledges financial support from a research grant from Saint Petersburg State University (Grant No. 94033852).

[1] M. B. Panish and M. Ilegams, *Progress in Solid State Chemistry* (Pergamon, New York, 1972), Vol. 7.

[2] V. Tomashyk, *Ternary Alloys Based on III-V Semiconductors* (CRC, Boca Raton, FL, 2017).

[3] C.-Z. Ning, L. Dou, and P. Yang, Bandgap engineering in semiconductor alloy nanomaterials with widely tunable compositions, Nat. Rev. Mater. **2**, 17070 (2017).

[4] K. Kaiiyama, Vapor pressure dependence of the relative composition of III-V mixed crystals in vapor phase epitaxy, J. Electrochem. Soc. **123**, 423 (1976).

[5] Y. Kumagai, J. Kikuchi, Y. Matsuo, Y. Kanagawa, K. Tanaka, and A. Koukitu, Thermodynamic analysis of InN and $In_xGa_{1-x}N$ MOVPE using various nitrogen sources, J. Cryst. Growth **272**, 341 (2004).

[6] J. Adhikari and D. Kofke, Molecular simulation study of miscibility of ternary and quaternary InGaAlN alloys, J. Appl. Phys. **95**, 6129 (2004).

[7] Y. Kanagawa, T. Ito, Y. Kumagai, and A. Koukitu, Thermodynamic study on compositional instability of InGaN/GaN and InGaN/InN during MBE, Appl. Surf. Sci. **216**, 453 (2003).

[8] Z. Ye, Y. Shu, X. Cao, L. Gong, B. Pi, J. Yao, X. Xing, and J. Xu, Thermodynamic analysis of growth of ternary III-V semiconductor materials by molecular-beam epitaxy, Trans. Nonferrous Met. Soc. China **21**, 146 (2011).

[9] L. Samuelson, P. Omling, and H. G. Grimmeiss, Alloying mechanisms in MOVPE $GaAs_{1-x}P_x$, J. Cryst. Growth **61**, 425 (1983).

[10] R. M. Biefeld, The preparation of InSb and $InAs_{1-x}Sb_x$ by metalorganic chemical vapor deposition, J. Cryst. Growth **75**, 255 (1986).

[11] T. Fukui and Y. Horikoshi, Organometallic VPE growth of $InAs_{1-x}Sb_x$ on InAs, Jpn. J. Appl. Phys. **19**, L53 (1980).

[12] W.-K. Chen and M.-T. Chin, Influence of thermodynamic factors on growth of $AlAs_{1-x}Sb_x$ Alloys, Jpn. J. Appl. Phys. **33**, 1370 (1994).

[13] B. W. Liang and C. W. Tu, A kinetic model for As and P incorporation behaviors in GaAsP grown by gas-source molecular beam epitaxy, J. Appl. Phys. **74**, 255 (1993).

[14] A. Y. Egorov, A. R. Kovsh, V. M. Ustinov, A. E. Zhukov, P. S. Kop'ev, and C. W. Tu, A thermodynamic analysis of the growth of III-V compounds with two volatile group V elements by molecular-beam epitaxy, J. Cryst. Growth **188**, 69 (1998).

[15] L. C. Chuang, M. Moewe, M. C. Chase, N. P. Kobayashi, C. Chang-Hasnain, and S. Crankshaw, Critical diameters for III-V nanowires grown on lattice-mismatched substrates, Appl. Phys. Lett. **90**, 043115 (2007).

[16] F. Glas, Critical dimensions for the plastic relaxation of strained axial heterostructures in free-standing nanowires, Phys. Rev. B **74**, 121302(R) (2006).

[17] V. G. Dubrovskii, N. V. Sibirev, X. Zhang, and R. A. Suris, Stress-driven nucleation of three-dimensional crystal islands: From quantum dots to nanoneedles, Cryst. Growth Des. **10**, 3949 (2010).

[18] P. C. McIntyre and A. Fontcuberta i Morral, Semiconductor nanowires: To grow or not to grow?, Mater. Today Nano **9**, 100058 (2020).

[19] V. G. Dubrovskii and F. Glas, Vapor-liquid-solid growth of semiconductor nanowires, in *Fundamental Properties of Semiconductor Nanowires*, edited by N. Fukata and R. Rurali (Springer, New York, 2020).

[20] P. K. Mohseni, A. Behnam, J. D. Wood, C. D. English, J. W. Lyding, E. Pop, and X. Li, $In_xGa_{1-x}As$ nanowire growth on graphene: Van der Waals epitaxy induced phase segregation, Nano Lett. **13**, 1153 (2013).

[21] M. Zeghouane, G. Avit, Y. André, C. Bougerol, Y. Robin, P. Ferret, D. Castelluci, E. Gil, V. G. Dubrovskii, H. Amano, and A. Trassoudaine, Compositional control of homogeneous InGaN nanowires with the In content up to 90%, Nanotechnology **30**, 044001 (2019).

[22] M. Heiss, A. Gustafsson, S. Conesa-Boj, F. Peiro, J. R. Morante, G. Abstreiter, J. Arbiol, L. Samuelson, and A. Fontcuberta i Morral, Catalyst-free nanowires with axial $In_xGa_{1-x}As$/GaAs heterostructures, Nanotechnology **20**, 075603 (2009).

[23] A. C. Farrell, W. J. Lee, P. Senanayake, M. A. Haddad, S. V. Prikhodko, and D. L. Huffaker, High-quality InAsSb nanowires grown by catalyst-free selective-area metal-organic chemical vapor deposition, Nano Lett. **15**, 6614 (2015).

[24] Q. D. Zhuang, E. A. Anyebe, R. Chen, H. Liu, A. M. Sanchez, M. K. Rajpalke, T. D. Veal, Z. M. Wang, Y. Z. Huang, and H. D. Sun, Sb-induced phase control of InAsSb nanowires grown by molecular beam epitaxy, Nano Lett. **15**, 1109 (2015).

[25] I. Isakov, M. Panfilova, M. J. L. Sourribes, V. Tileli, A. E. Porter, and P. A. Warburton, $InAs_{1-x}P_x$ nanowires grown by catalyst-free molecular-beam epitaxy, Nanotechnology **24**, 085707 (2013).

[26] C. S. Jung, H. S. Kim, G. B. Jung, K. J. Gong, Y. I. Cho, S. Y. Jang, C. H. Kim, C. Lee, and J. Park, Composition and phase tuned InGaAs alloy nanowires, J. Phys. Chem. **115**, 7843 (2011).

[27] D. Jacobsson, J. M. Persson, D. Kriegner, T. Etzelstorfer, J. Wallentin, J. B. Wagner, J. Stangl, L. Samuelson, K. Deppert, and M. T. Borgstrom, Particle-assisted $Ga_xIn_{1-x}P$ nanowire growth for designed bandgap structures, Nanotechnology **23**, 245601 (2012).

[28] S. Hertenberger, S. Funk, K. Vizbaras, A. Yadav, D. Rudolph, J. Becker, S. Bolte, M. Döblinger, M. Bichler, G. Scarpa, P. Lugli, I. Zardo, J. J. Finley, M.-C. Amann, G. Abstreiter, and G. Koblmüller, High compositional homogeneity in In-rich

InGaAs nanowire arrays on nanoimprinted SiO_2/Si (111), Appl. Phys. Lett. **101**, 043116 (2012).

[29] J. Wu, M. Borg, D. Jacobsson, K. A. Dick, and L. E. Wernersson, Control of composition and morphology in InGaAs nanowires grown by metalorganic vapor phase epitaxy, J. Cryst. Growth **383**, 158 (2013).

[30] A. S. Ameruddin, H. A. Fonseka, P. Caroff, J. Wong-Leung, Roy L. M. Ophet Veld, J. L. Boland, M. B. Johnston, H. H. Tan, and C. Jagadish, $In_xGa_{1-x}As$ nanowires with uniform composition, pure wurtzite crystal phase and taper-free morphology, Nanotechnology **26**, 205604 (2015).

[31] A. S. Ameruddin, P. Caroff, H. H. Tan, C. Jagadish, and V. G. Dubrovskii, Understanding the growth and composition evolution of gold-seeded ternary InGaAs nanowires, Nanoscale **7**, 16266 (2015).

[32] G. Priante, F. Glas, G. Patriarche, K. Pantzas, F. Oehler, and J. C. Harmand, Sharpening the interfaces of axial heterostructures in self-catalyzed AlGaAs nanowires: Experiment and theory, Nano Lett. **16**, 1917 (2016).

[33] V. G. Dubrovskii, I. V. Shtrom, R. R. Reznik, Yu. B. Samsonenko, A. I. Khrebtov, I. P. Soshnikov, S. Rouvimov, N. Akopian, T. Kasama, and G. E. Cirlin, Origin of spontaneous core-shell AlGaAs nanowires grown by molecular beam epitaxy, Cryst. Growth Des. **16**, 7251 (2016).

[34] A. I. Persson, M. T. Bjork, S. Jeppesen, J. B. Wagner, L. R. Wallenberg, and L. Samuelson, $InAs_{1-x}P_x$ nanowires for device engineering, Nano Lett. **6**, 403 (2006).

[35] B. M. Borg, K. A. Dick, J. Eymery, and L.-E. Wernersson, Enhanced Sb incorporation in InAsSb nanowires grown by metalorganic vapor phase epitaxy, Appl. Phys. Lett. **98**, 113104 (2011).

[36] X. Yuan, P. Caroff, J. Wong-Leung, H. H. Tan, and C. Jagadish, Controlling the morphology, composition and crystal structure in gold-seeded $GaAs_{1-x}Sb_x$ nanowires, Nanoscale **7**, 4995 (2015).

[37] Y. Zhang, A. M. Sanchez, Y. Sun, J. Wu, M. Aagesen, S. Huo, D. Kim, P. Jurczak, X. Xu, and H. Liu, Influence of droplet size on the growth of self-catalyzed ternary GaAsP nanowires, Nano Lett. **16**, 1237 (2016).

[38] V. Zannier, F. Rossi, V. G. Dubrovskii, D. Ercolani, S. Battiato, and L. Sorba, Nanoparticle stability in axial InAs−InP nanowire heterostructures with atomically sharp interfaces, Nano Lett. **18**, 167 (2018).

[39] V. G. Dubrovskii, Understanding the vapor-liquid-solid growth and composition of ternary III-V nanowires and nanowire heterostructures, J. Phys. D **50**, 453001 (2017).

[40] M. Ghasemi, E. D. Leshchenko, and J. Johansson, Assembling your nanowire: An overview of composition tuning in ternary III-V nanowires, Nanotechnology **32**, 072001 (2021).

[41] F. Glas, Comparison of modeling strategies for the growth of heterostructures in III-V nanowires, Cryst. Growth Des. **17**, 4785 (2017).

[42] V. G. Dubrovskii, A. A. Koryakin, and N. V. Sibirev, Understanding the composition of ternary III-V nanowires and axial nanowire heterostructures in nucleation-limited regime, Mat. Design **132**, 400 (2017).

[43] J. Johansson and M. Ghasemi, Composition of gold alloy seeded InGaAs nanowires in the nucleation limited regime, Cryst. Growth Des. **17**, 1630 (2017).

[44] V. G. Dubrovskii, Compositional control of gold-catalyzed ternary nanowires and axial nanowire heterostructures based on $IIIP_{1-x}As_x$, J. Cryst. Growth **498**, 179 (2018).

[45] E. D. Leshchenko, M. Ghasemi, V. G. Dubrovskii, and J. Johansson, Nucleation-limited composition of ternary III-V nanowires forming from quaternary gold based liquid alloys, Cryst. Eng. Comm. **20**, 1649 (2018).

[46] V. G. Dubrovskii, Fully analytical description for the composition of ternary vapor-liquid-solid nanowires, Cryst. Growth Des. **15**, 5738 (2015).

[47] J. Johansson and M. Ghasemi, Kinetically limited composition of ternary III-V nanowires, Phys. Rev. Mater. **1**, 040401(R) (2017).

[48] E. D. Leshchenko and J. Johansson, Role of thermodynamics and kinetics in the composition of ternary III-V nanowires, Nanomaterials **10**, 2553 (2020).

[49] E. D. Leshchenko and V. G. Dubrovskii, Kinetic modeling of interfacial abruptness in axial nanowire heterostructures, Nanotechnology **34**, 065602 (2023).

[50] V. G. Dubrovskii and E. D. Leshchenko, Kinetically controlled composition of III-V ternary nanostructures, Phys. Rev. Mater. **7**, 056001 (2023).

[51] D. McLean, *Grain Boundaries in Metals* (Oxford University, New York, 1957).

[52] T. Fukui and Y. Horikoshi, InAsSbP-InAs superlattice grown by organometallic VPE method, Jpn. J. Appl. Phys. **19**, L551 (1980).

[53] W.-N. Du, X.-Y. Wang X.-G.Yang, H.-Y. Pan, H.-M. Ji, S. Luo, T. Yang, and Z.-G. Wang, The self-seeded growth of InAsSb nanowires on silicon by metal-organic vapor phase epitaxy, J. Cryst. Growth **396**, 33 (2014).

[54] C. Himwas, S. Collin, P. Rale, N. Chauvin, G. Patriarche, F. Oehler, F. H. Julien, L. Travers, J. C. Harmand, and M. Tchernycheva, In situ passivation of GaAsP nanowires, Nanotechnology **28**, 495707 (2017).

[55] Y. Zhang, M. Aagesen, J. V. Holm, H. I. Jørgensen, J. Wu, and H. Liu, Self-catalyzed GaAsP nanowires grown on silicon substrates by solid-source molecular beam epitaxy, Nano Lett. **13**, 3897 (2013).

[56] I. Ansara, C. Chatillon, H. L. Lukas, T. Nishizawa, H. Ohtani, K. Ishida, M. Hillert, B. Sundman, B. B. Argent, A. Watson, T. Chart, and T. Anderson, A binary database for III-V compound semiconductor systems, Calphad **18**, 177 (1994).

[57] F. Glas, M. R. Ramdani, G. Patriarche, and J. C. Harmand, Predictive modeling of self-catalyzed III-V nanowire growth, Phys. Rev. B **88**, 195304 (2013).